Chemical Engineering Journal Advances 24 (2025) 100896

Contents lists available at ScienceDirect

Chemical Engineering Journal Advances

journal homepage: www.sciencedirect.com/journal/chemical-engineering-journal-advances

Recovery of organic electrolyte solvents from spent perforated Li-ion cells using a low-temperature vacuum-assisted distillation process

Tendai Tawonezvi [a,*], Anele Sinto [a,b], Dorcas Zide [a,b], Myalelo Nomnqa [c], Bernard J. Bladergroen [a]

[a] South African Institute for Advanced Materials Chemistry (SAIAMC), University of the Western Cape, Robert Sobukwe Road, Bellville, Cape Town 7535, South Africa
[b] Department of Chemistry, Cape Peninsula University of Technology (CPUT), Symphony Way, Bellville, Cape Town 7535, South Africa
[c] Department of Chemical Engineering, Cape Peninsula University of Technology (CPUT), Symphony Way, Bellville, Cape Town 7535, South Africa

ARTICLE INFO

Keywords:
Lithium-ion batteries
Recycling process
Vacuum-thermal treatment
Condensation
Electrolyte solvent

ABSTRACT

Electrolyte solvent recovery is rarely addressed in current state-of-the-art lithium-ion battery (LiB) recycling processes, even though electrolytes are flammable, toxic, and hazardous. In conventional recycling processes, electrolytes typically evaporate or decompose uncontrollably during pre-treatment steps such as shredding, leading to both safety risks and environmental damage. To overcome these limitations, we investigated a controlled electrolyte solvent recovery process using mild-temperature vacuum distillation on perforated, intact batteries rather than shredded material. This method enabled safe handling and minimised uncontrolled emissions during pre-treatment. Analysis results demonstrate a successful 84 % recovery of the major electrolyte solvents, dimethyl carbonate (DMC), ethyl methyl carbonate (EMC), and ethylene carbonate (EC), after 300 min of thermal-vacuum treatment at 110 °C and 80 mBar vacuum pressure. Decomposition products of Lithium Hexafluorophosphate ($LiPF_6$), which include hydrogen fluoride (HF) and phosphoryl fluoride (POF_3), were not identified in the exhaust gas, and the scrubber solution remained neutral during operation. These results demonstrate that thermal treatment below 110 °C is a non-complex, feasible, and environmentally friendly process for recovering electrolyte solvents prior to metal recovery, addressing a major gap in current LiB recycling processes.

Introduction

The first commercial rechargeable lithium-ion battery (LiB) was introduced by Sony and Asahi Kasei in 1991[1]. Since then, LiB chemistries such as NMC, LCO, LMO, NCA, and LFP have been developed and refined to enhance energy and power density, cycle life, and safety. Despite differences in material composition and design, typical LiBs consist of a layered structure anode (15–25 wt %), separator (4–10 wt %), transition metal oxide cathode (25–35 wt %), and a liquid electrolyte (10–20 wt %) [2,3]. While these components contribute relatively evenly to battery mass, the economic value is heavily concentrated in the active cathode materials, typically consisting of cobalt (Co), nickel (Ni), lithium (Li), and copper (Cu), which has led to recycling practices that prioritise metal recovery [4].

Driven by rising environmental concerns and raw material demand, the European Commission has proposed revisions to the 2006 battery directive, introducing higher recycling efficiency targets (65 wt % by 2025 and 70 wt % by 2030) [5]. However, these targets are difficult to meet without the recovery of lower-value but environmentally impactful components, such as the electrolyte and separator. Due to the complex architecture of LiBs, comprehensive recycling typically requires multi-step processes, including mechanical dismantling, thermal treatment, and hydrometallurgy. Pyrolysis, often conducted at ~550 °C to remove binders like PVDF and free active materials, is commonly used but leads to the decomposition of electrolyte salts or uncontrolled evaporation of volatile organic electrolyte solvents [6,7]. This not only causes material losses but also releases toxic and corrosive byproducts into the environment.

LiB electrolytes typically contain a lithium salt, most commonly $LiPF_6$, dissolved in carbonate-based solvents such as dimethyl carbonate (DMC), ethyl methyl carbonate (EMC), diethyl carbonate (DEC), ethylene carbonate (EC), and propylene carbonate (PC) [7]. These electrolyte solvents are flammable and volatile, and exposure of the electrolyte salt to heat or moisture can generate harmful substances such

* Corresponding author.
E-mail address: tendaitawonezvi@yahoo.com (T. Tawonezvi).

https://doi.org/10.1016/j.ceja.2025.100896

Available online 3 October 2025

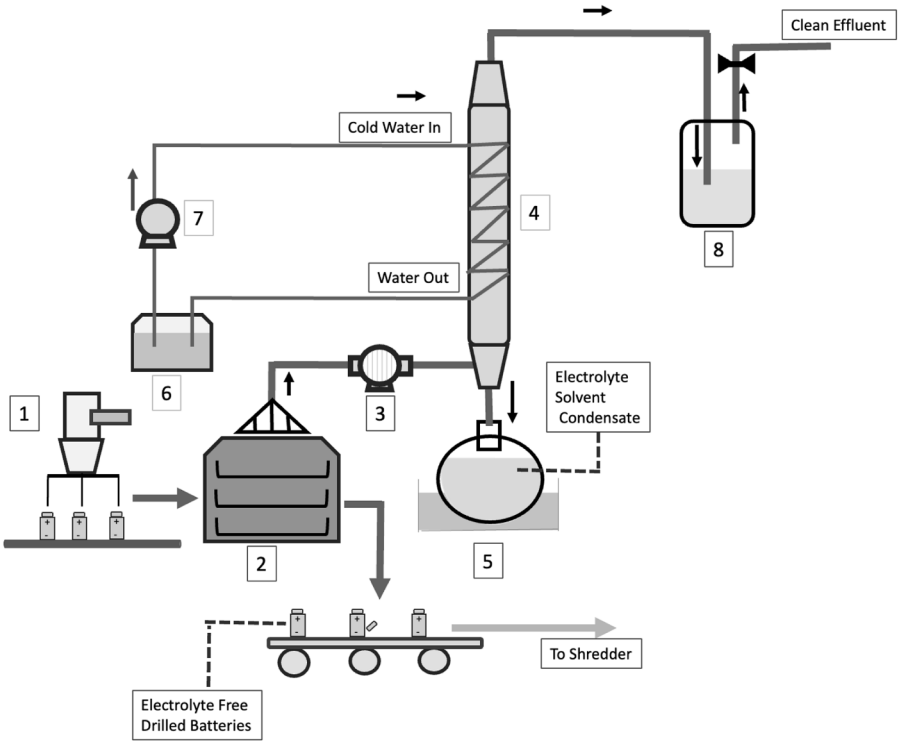

Fig. 1. Process flow diagram of the experimental set-up of the vacuum-assisted distillation process for electrolyte solvent recovery, (1) battery drilling table, (2) vacuum oven, (3) vacuum pump, (4) condensation column, (5) collection vessel, (6) cold water bath, (7) peristaltic pump and (8) scrubber unit.

as hydrogen fluoride (HF) and phosphoryl fluoride (POF_3), posing risks to both human and environmental health. Residual electrolytes also complicate the treatment of separators, increasing costs and handling complexity.

In response, several studies have explored methods to extract and recover electrolytes prior to high-temperature or mechanical processing. Techniques include supercritical CO_2 extraction, solvent extraction, and low-temperature volatilisation. For instance, Grützke et al. utilised a supercritical helium-assisted CO_2 system to extract solvents and $LiPF_6$ from jelly rolls, though the process had long extraction times and low EC and salt recovery[8]. Improvements using flow-through systems with co-solvents showed better yields but were highly sensitive to operating parameters [8]. Similarly, Mu et al. [9] demonstrated effective recovery of electrolyte components from separators using a transcritical CO_2 method. Aqueous-based extractions have also shown promise; He et al. [10] reported high recovery using an aqueous exfoliating and extracting solution, though this required manual stripping of components, increasing exposure risks and processing complexity. Other studies have applied low-temperature volatilisation (e.g., at 120 °C) but lacked detailed analysis of recovered products and gaseous emissions [11,12].

While conventional methods advanced electrolyte recovery, they remain constrained by key limitations. Many rely on utilising elevated processing temperatures, pressures and/or pre-shredded LiBs, where mechanical heat and friction induce substantial electrolyte solvent loss prior to recovery. This not only reduces recovery efficiency but also leads to uncontrolled emissions of hazardous gaseous by-products.

In this study, we introduce a mild-temperature, vacuum-assisted distillation technique applied directly to intact perforated LiBs, rather than shredded or fully dismantled LiB components. This configuration mitigates premature solvent volatilisation during mechanical processing and reduces the occupational risks associated with manual handling in aqueous-based recovery methods. The application of vacuum conditions decreases the boiling points of carbonate-based solvents, enabling efficient recovery within the 70–120 °C range. Operating within this thermal window avoids separator melting (~135–160 °C) and suppresses the formation of $LiPF_6$ degradation products, which begin to evolve at approximately 128.5 °C [13,14].

Furthermore, in contrast to prior volatilisation studies that lacked detailed characterisation, the present work provides a quantitative and qualitative assessment of solvent recovery yields and confirms the absence of deleterious $LiPF_6$ decomposition products. These outcomes collectively distinguish the proposed methodology from existing approaches and underscore its potential for scalable industrial implementation. Unlike prior volatilisation studies lacking quantitative and qualitative analysis, the presented method provides measured recovery yields and confirms the absence of harmful decomposition products, demonstrating a non-complex, safe, and potentially scalable approach for industrial LiB recycling.

Attenuated total reflection Fourier-transform infrared spectroscopy (ATR-FTIR) and XRD were used to characterise the recovered solvents, while ex-situ ion chromatography (IC) was employed to monitor exhaust gases and identify potential degradation products. The results further underscores that low-temperature vacuum distillation provides a simple, safe, and scalable method for recovering key electrolyte solvents, such as DMC, EMC, and EC, prior to downstream metal recovery. This approach offers operational simplicity, feasibility for industrial applications, and significant environmental benefits by minimising hazardous emissions and improving the overall recycling efficiency of LiBs.

Materials and methods

Materials

Spent lithium-ion battery prismatic cells (LFP) from a retired 3.7 kWh energy storage system were obtained from Solar MD, South Africa and used in this study. NMC battery shreds were sourced from the uYilo eMobility Institute at Nelson Mandela University, South Africa. Commercial LiB electrolyte purchased from Dongguan Shanshan `Battery Materials Co., Ltd, China was used in this study. HNO_3 (>65 %), acetone (>95 %) were purchased from Merck Millipore, USA.

Table 1
Calculated boiling points of common electrolyte solvents at atmospheric pressure (1000 mbar) and reduced pressure (80 mbar), based on Antoine equation-derived vapour pressure plots.

	Boiling point at 1000 mBar (°C)	Boiling point at 80 mBar (°C)	In-house electrolyte solvent composition (v/v%)
DMC	90	22.5	33.3
DEC	125	25	0
EC	243	108	33.3
PC	242	88	0
EMC	110	30	33.3

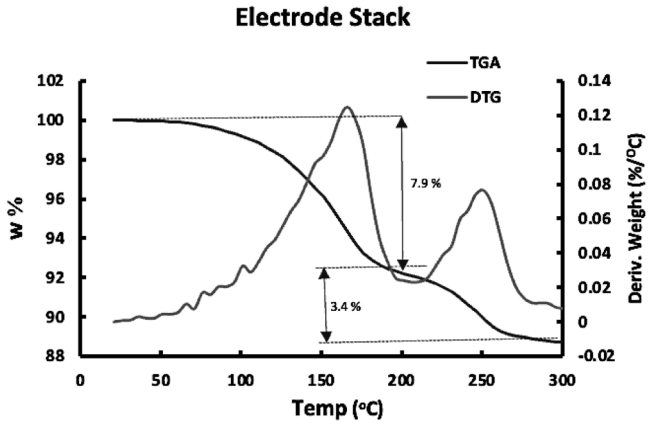

Fig. 2. TG (blue) and DTG (red) curves of the electrode stack of a freezer-stored LiB cell.

Experimental methods

Sample preparation

Discharged LFP prismatic cells were stored at 4 °C for two days to minimise the evaporation of volatile electrolyte solvents prior to opening. The cells were discharged through a low-resistance rod-shaped wire with a resistance of 50 mΩ, which acts as a passive resistive load, converting the electrical energy into heat via Joule heating. To monitor the discharge process, a precision shunt resistor (0.96 mΩ) was placed in series with the load (in parallel with a multimeter), and the voltage drop across it was recorded using a multimeter to calculate the real-time current via Ohm's law. The prismatic cells were placed on an aluminium metal sheet in direct contact with the oven's heating elements. The high thermal conductivity of aluminium facilitated rapid and uniform heat transfer to the cells, enhancing the evaporation rate of the volatile solvents. Two holes were punctured on the top surface near the terminals of the discharged prismatic cells using an 8 mm drill bit, and the electrode stack, comprising multiple layers of anode, separator, and cathode, was only cut open to free the electrode stack after vacuum-assisted distillation to examine the remaining deposits on the electrodes. For each thermal treatment experiment, rectangular cells (9 × 6 cm, weighing 1900.07 ± 95 *g*) were used. Between experiments, the remaining electrode stack was stored in a sealed plastic bag at 4 °C.

Experimental method

A schematic process flow diagram of the electrolyte solvent recovery procedure is shown in is illustrated in Fig. 1.

The thermal treatment was performed using a vacuum oven (Binder VD53, Germany) operated under reduced pressure conditions (80 mBar). The outlet of the vacuum chamber was connected to a vacuum pump (Chem Vac 400, Sigma-Aldrich), which facilitated the removal of evolved gases during heating. These gases passed through a condensation column maintained at 15 °C during treatment and 35 °C for 5 min post-treatment via a circulating water bath to melt any EC deposit and ensure maximum recovery. Condensable vapours were collected in a vial positioned beneath the column. Upstream of the condensation column, a gas-washing vessel containing 150 mL of Milli-Q water was installed to trap volatile water-soluble compounds to prevent their emission into the atmosphere. This configuration enabled effective condensation and capture of thermally generated volatile species without the need for a carrier gas such as nitrogen.

The oven temperatures used were 50 °C, 70 °C, 90 °C, 110 °C, and 120 °C, monitored via a thermocouple connected to a data logger (TC-08, Pico Technology). Each battery sample was placed on an aluminium metal sheet plate (inside the vacuum oven) to allow for effective heat transfer. After 300 min of thermal treatment, the battery was removed from the oven at the operating temperature and cooled to room temperature. The sample mass was recorded under ambient conditions using a precision balance, both before and after thermal treatment, to determine the extent of mass loss during the process.

Each temperature condition was tested in triplicate in random order. In all the replicates, the recovered condensate was analysed using ATR-FTIR. In all runs, exhaust gas was bubbled through the gas washing vessel prior to atmospheric release. The washing water was analysed using ion chromatography (IC), and its pH was measured. Any solid crystals (formed in or on the battery) from the process were collected

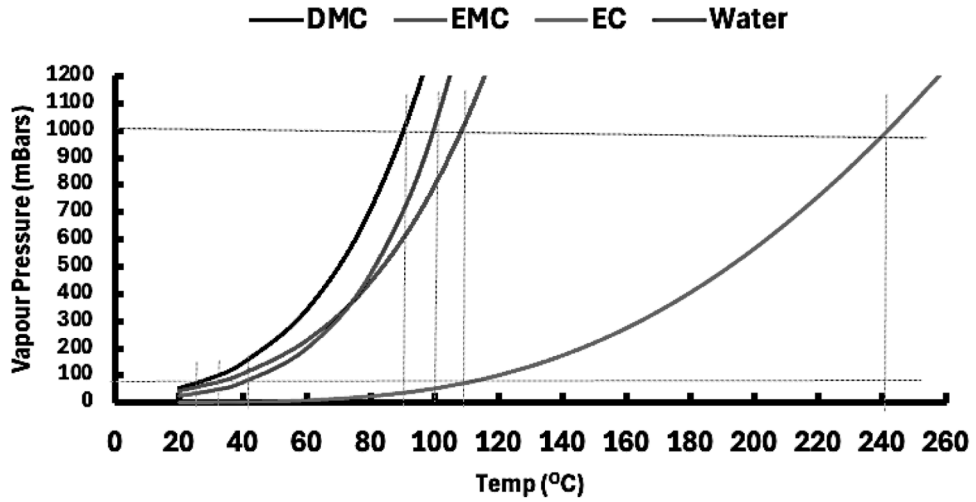

Fig. 3. Boiling point determination at 80 mBar and 1000 mBar using the Antoine equation. The plot shows the relationship between vapour pressure as a function of temperature for Water, EC, DMC and EMC, with the boiling temperature corresponding to the intersection at 80 mBar (60 mmHg).

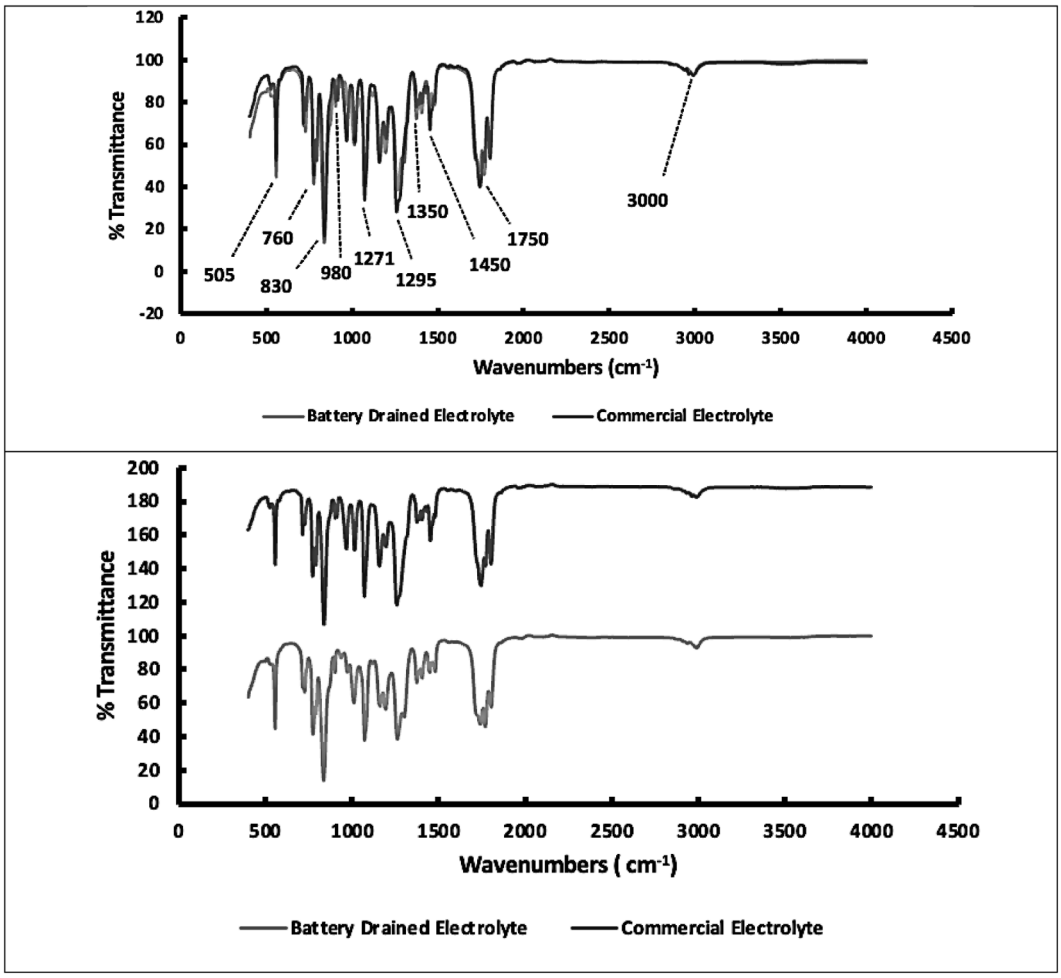

Fig. 4. FT-IR spectra of the battery-drained electrolyte and commercial electrolyte.

after cooling and analysed via ATR-FTIR, XRD, and ICP-OES.

Measurement and characterisation

TGA was performed using a Q500 instrument (TA Instruments) from 20 °C to 300 °C at a nitrogen flow rate of 100 mL/min. A heating rate of up to 5 °C/min was used, with a high-resolution sensitivity of 4.0 and resolution of 5.0, enabling automated adjustment of the heating rate based on weight change. Sample weight was 20.99 ± 0.01 mg.

The exhaust gases were monitored by in-situ FTIR spectroscopy (Spectrum Two, Perkin Elmer) from 4000 cm^{-1} to 900 cm^{-1}, resolution 4 cm^{-1}, scan time 40 s (~12 scans). Pure nitrogen at 340 mL/min in an empty run served as the background. Reference FTIR spectra for EC, DMC and EMC were recorded by evaporating small droplets inside the gas cell. The FTIR spectra of the evolving gases were analysed for composition and peak evolution over the 180-minute reaction.

Collected crystalline condensates were characterised by ATR-FTIR in the range of 4000–450 cm^{-1} with 2 cm^{-1} resolution over 32 scans. Crystalline phases were identified using X-ray diffraction (Bruker D8 Advance). Condensates were then dissolved in 5 mL of 0.5 M HNO_3, filtered, and analysed for elemental content using ICP-OES (iCAP PRO, ThermoFisher Scientific).

Calculation

The weight loss (%) from thermal treatment was calculated as:

$$\textit{Cell Weight Loss}\ (\%) = \left(1 - \frac{m_t}{m_i}\right) \tag{1}$$

Where m_i is the initial mass of the sample and m_t is the final mass after treatment.

The solvent recovery (%) from thermal treatment was calculated as:

$$\textit{Solvent Recovery}\ (\%) = \frac{\rho V_t}{(m_i - m_t)} \tag{2}$$

Where ρ is the density of the electrolyte solvent mixture, V_t is the actual electrolyte solvent volume collected, m_i is the initial mass of the battery sample, and m_t is the final battery mass after treatment.

To account for baseline solvent loss under ambient conditions, a preliminary control experiment was conducted at room temperature in a fume hood. The sample was exposed to ambient airflow and periodically weighed over time to quantify evaporative mass loss. This control provided a reference against which mass changes under elevated temperatures or varied conditions could be compared.

Scrubber solution analysis

Gas washing water samples were diluted 1:30 with Milli-Q water and injected (20 µL) into a Dionex IonPac AG4ASC column (4 × 50 mm) for anion analysis by IC using a carbonate eluent (1.7 mM $NaHCO_3$, 1.8 mM Na_2CO_3). Milli-Q water served as the background. Major and minor element composition analysis of the samples was measured on Agilent 8800. QQQ ICP MS instrument.

Results and discussion

Material characterisation

TGA was conducted on the discharged spent LiB cathode electrode

Table 2
Summary of the characteristic peaks used for the assignments of the electrolyte FT-IR spectrum between 2000 cm^{-1} and 900 cm^{-1}. ν, δ, a and s represent stretching, bending, asymmetric and symmetric deformation.

Wavenumber (cm^{-1})	DMC [19]	EC [20]	EMC [21]	$LiPF_6$ [22,23]
~500	–	–	–	F–P–F bending ($LiPF_6$)
720–760	CH_3 rocking	–	CH_3 rocking	Ring deformation / P–O ring modes
840–880	–	–	–	Possible overtones / weak PF interactions
980–990	–	–	–	P–F stretching ($LiPF_6$)
990–1060	C–O asymmetric stretch (O–CH_3)	Ring C–O stretch	C–O stretch (linear)	Minor overlap with PF stretches
1005–1150	C–O–C symmetric stretch	C–O–C ring symmetric stretch	C–O–C symmetric stretch	Minor overlap with POF_3 stretch (1014 cm^{-1})
1050	–	–	–	POF_3 asymmetric stretch
1220–1280	CH_3 rocking, C–O bending	–	CH_3 rocking	–
1340–1380	CH_3 bending	–	CH_3 bending	–
1430–1480	–	CH_2 bending (weak)	CH_2 bending (ethyl)	–
1650	–	–	–	CH_2/CH_3 deformation (from residual organics)
1700–1780	*C = O* stretch (non-ring carbonyl)	*C = O* stretch (cyclic carbonate)	*C = O* stretch (non-ring)	–
2850–2950	CH_3 symmetric/ asymmetric stretch	–	CH_3/CH_2 symmetric/ asymmetric stretch	–
3200–3600	– (only if moisture present)	O–H stretch (moisture or HF)	O–H stretch (moisture)	O–H stretch from trace H_2O or HF

stack to characterise the thermal behaviour of the electrolyte solvent mixture and guide temperature selection for low-temperature vacuum-assisted distillation.

The sample (0.25 *g*), stored at –18 °C prior to testing to minimise solvent loss, exhibited a total mass loss of approximately 11.3 wt % over the temperature range of 20–300 °C. The majority of this loss (7.9 wt %) occurred between 20 °C and 150 °C, as shown in the TGA curve. This initial weight loss is primarily attributed to the evaporation of low-boiling electrolyte solvents such as dimethyl carbonate (DMC, boiling point ~90 °C) and diethyl carbonate (DEC, boiling point ~110 °C), both of which are common constituents in LiB electrolytes [15–17].

Another reaction may occur between approximately 150 °C and 180 °C, corresponding to the onset of $LiPF_6$ decomposition, which is known to initiate within this temperature range and yields products such as PF_5 and LiF [18]. A second, smaller DTG peak, aligning with 3.4 % mass loss, was detected between 200 °C and 250 °C, which aligns with the boiling point of ethylene carbonate (EC, ~243–248 °C). This feature is attributed to the volatilisation and/or thermal decomposition of EC, as well as the breakdown of other high-boiling electrolyte components, the solid–electrolyte interphase (SEI), and conductive carbon additives.

No significant DTG peaks were observed above 260 °C, indicating the absence of further thermal decomposition processes within the studied range. This supports the selection of 260 °C as a conservative upper thermal treatment limit under ambient pressure conditions. However, the application of a vacuum atmosphere effectively lowers the boiling points of the electrolyte solvents. As summarised in Table 1, the boiling points of DMC, EC, and EMC under vacuum are reduced to approximately 22.5 °C, 108 °C, and 30 °C, respectively. Antoine equation extrapolations further suggest that an upper thermal treatment limit of 120 °C under vacuum conditions is appropriate to maximise solvent removal while minimising decomposition of electrode and electrolyte materials. Accordingly, intermediate process temperatures of 50 °C, 70 °C, 90 °C, 110 °C, and 120 °C were selected to coincide with the DTG maxima and ensure efficient solvent recovery with minimal degradation of the electrode structure.

Fig. 2

To assess the solvent composition and identify any other additives utilised in the electrolyte solution, ATR-FT-IR spectroscopy, presented in Fig. 3, was performed on the battery-drained electrolyte and pure commercial electrolyte sampled before the vacuum-assisted distillation process to recover electrolyte solvent (Fig. 4 and Table 2).

Spectra collected from the battery-drained electrolyte and commercial electrolyte before recovery operations revealed clear absorbance peaks characteristic of organic carbonate solvents commonly used in LiBs. Distinct peaks at 1780 cm^{-1} (C═O stretching), 1460 cm^{-1} (CH_3 symmetric deformation), and 1295 cm^{-1} (C–O stretching) were consistent with the presence of DMC, as previously reported in the literature [24,25].

EMC was identified by its characteristic C═O stretch at ~1770 cm^{-1} and CH_3/CH_2 deformation bands between 1340 and 1380 cm^{-1}, which align with published spectral data [26,27]. Though EC is less volatile and was not distinctly identified in TGA, it was detected via FTIR by its distinctive C═O stretching band in the range of 1800–1820 cm^{-1}, attributable to the cyclic carbonate structure [24].

In contrast, DEC, despite a massive mass loss within its decomposition temperature, was not detected in the FTIR spectra. Its absence may be due to rapid evaporation or insufficient concentration under the FTIR sampling conditions. DEC typically exhibits bands at 1760 cm^{-1} (C═O stretch) and 1270 cm^{-1} (C–O stretch), which were not observed in either the commercial or battery-drained electrolyte spectra. In addition to organic carbonates, $LiPF_6$, the commonly used lithium salt in commercial electrolytes, was identified in both electrolyte samples. Its presence was confirmed by strong FTIR absorbance peaks at approximately 980 cm^{-1} (P–F stretching) and 500 cm^{-1} (F–P–F bending), which are consistent with literature reports [22–29]. Minor peaks at 1050 cm^{-1} and 480 cm^{-1} were also observed and attributed to phosphoryl fluoride (POF_3), suggesting partial thermal or hydrolytic decomposition of $LiPF_6$.

Overall, the combined FTIR and TGA results indicate that the primary electrolyte solvent composition consists of EC as the cyclic carbonate and DMC and EMC as linear carbonates. The high volatility of DMC and EMC under nitrogen purge highlights the need to carefully control recovery conditions to minimise solvent loss and ensure efficient recovery of components.

Battery configuration in oven optimisation

The observed trend highlights the significant influence of battery orientation on the rate of solvent evaporation during vacuum-assisted thermal treatment. Two configurations were investigated, as shown in Fig. 5.

In the horizontal (flat) configuration, the large top-surface exposure of internal components immersed in electrolyte allows volatile solvents to escape more easily and, in some cases, physically splash out due to pressure and temperature changes. This resulted in a rapid initial mass loss of 7.5 % within just one hour, indicating efficient and immediate solvent removal. The total mass loss plateaued at 12.4 %, suggesting that most of the recoverable solvent was extracted early in the process. This configuration, therefore, offers a shorter processing time and lower

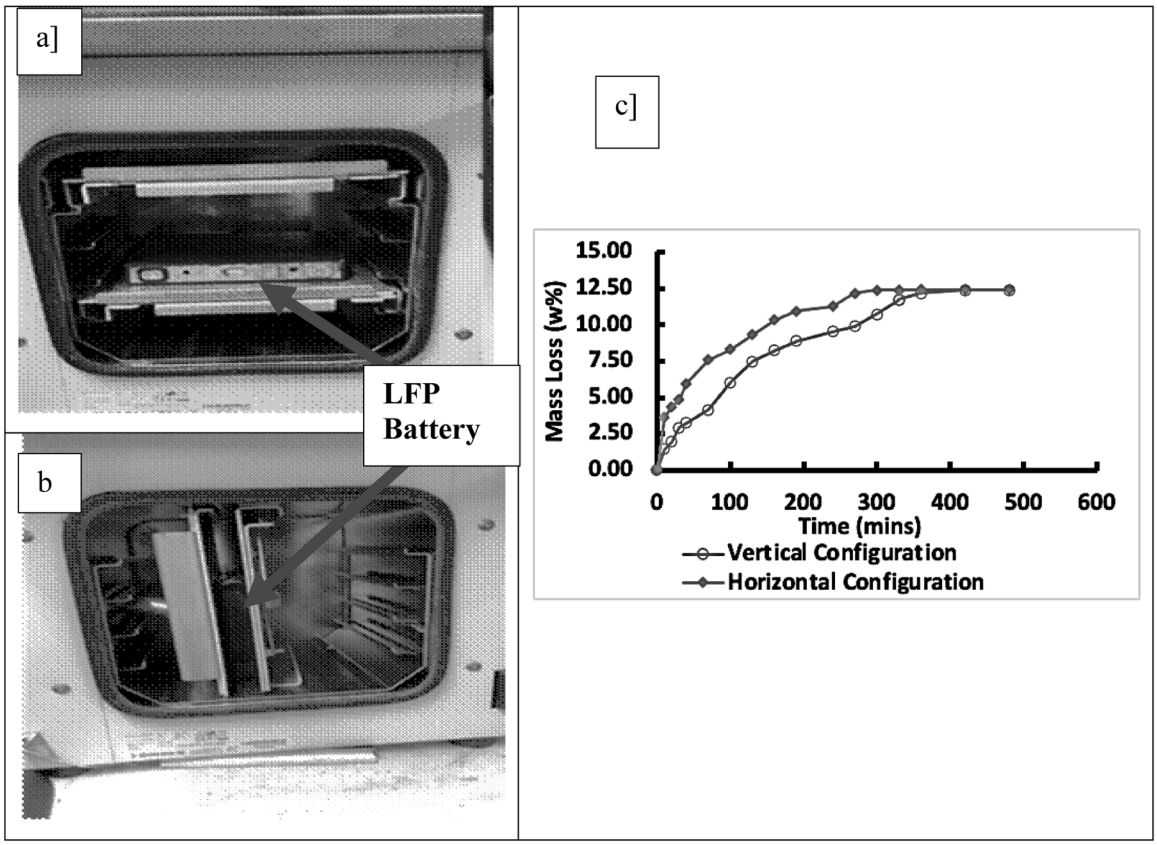

Fig. 5. (a) Horizontal configuration (flat) cell configuration in a vacuum oven, (b) vertical (Facing up) cell configuration in a vacuum oven and c) effect of cell configuration on the mass loss (%) at 80 mBar and 110 °C.

energy input, making it more efficient from an operational standpoint.

In contrast, the vertical (upright) configuration restricts the free movement and release of solvents, likely due to reduced battery-top surface exposure and less gravitational assistance for outward solvent migration. Although the final total mass loss was the same (12.3 %), it took 7 h to reach this point, with only an additional 4 % mass loss occurring after the first hour. This slower evaporation rate implies higher diffusion resistance within the confined battery structure in the upright orientation, despite the use of metal plates to enhance uniform heating.

Overall, the trend suggests that battery orientation strongly affects the fluid mass transfer dynamics of electrolyte solvents. While both methods achieve similar total solvent removal, the flat configuration is more time- and therefore energy-efficient, making it preferable for scalable recycling processes. However, the flat setup also carries a higher risk of uncontrolled solvent ejection, which emphasises the need for proper vapour capture and solvent containment systems to prevent environmental release and cross-contamination during processing.

Effect of temperature on weight loss

When an LFP battery is subjected to thermal treatment under vacuum conditions, the extent of weight loss is closely linked to temperature, reflecting a combination of solvent evaporation, electrolyte decomposition, and gas evolution.

Experimental results, in Fig. 6b, revealed that drilled battery samples consistently exhibited a higher percentage mass loss of 11.9 % during recovery treatments compared to 7.5 % observed in shredded samples, indicating a greater retention of electrolyte in the drilled configuration. This is attributed to the fact that shredding inherently leads to solvent loss, as the mechanical friction and the consequent disruption of the cell structure expose volatile components to air, allowing partial evaporation before any thermal or vacuum treatment is applied. In contrast, drilling minimises this exposure, preserving more of the original electrolyte within the sealed cell compartments while simultaneously reducing diffusion resistance during recovery.

As anticipated, the combination of vacuum and thermal treatment proved more effective than either approach alone, resulting in a higher mass loss of 11.9 % (Fig. 5a). While vacuum conditions lower the boiling points of the solvents, they do not provide sufficient thermal energy to drive off or decompose more stable electrolyte components. Likewise, thermal treatment under atmospheric pressure is limited by inefficient vapour removal, especially for high-boiling-point solvents such as ethylene carbonate (EC, ~243 °C). These results reinforce the understanding that neither vacuum nor heat alone is sufficient for the complete removal of electrolyte species, particularly those that are strongly retained within the electrode structure or confined within the cell architecture.

Additionally, these temperatures are insufficient to decompose thermally stable salts like $LiPF_6$ or affect the structural integrity of cathode materials such as $LiFePO_4$ (LFP) [13]. Only surface-adsorbed or loosely bound residues are removed under these conditions. In contrast, as shown in Fig. 6c, treatments at higher temperatures (>90 °C), especially under vacuum, result in considerable mass loss driven by multiple mechanisms. The increased thermal energy raises the vapour pressure of the solvents, promoting their evaporation. At the same time, $LiPF_6$ begins to decompose, generating volatile byproducts such as PF_5 and HF, which escape the system and contribute to the mass loss [30]. Vacuum enhances this process by reducing the ambient pressure, thereby lowering the boiling points of all solvent species and facilitating their removal even at moderate temperatures.

However, aggressive vacuum–thermal (130 °C) conditions can also lead to decomposition of non-electrolyte components such as polymeric binders or separators, releasing additional low-molecular-weight

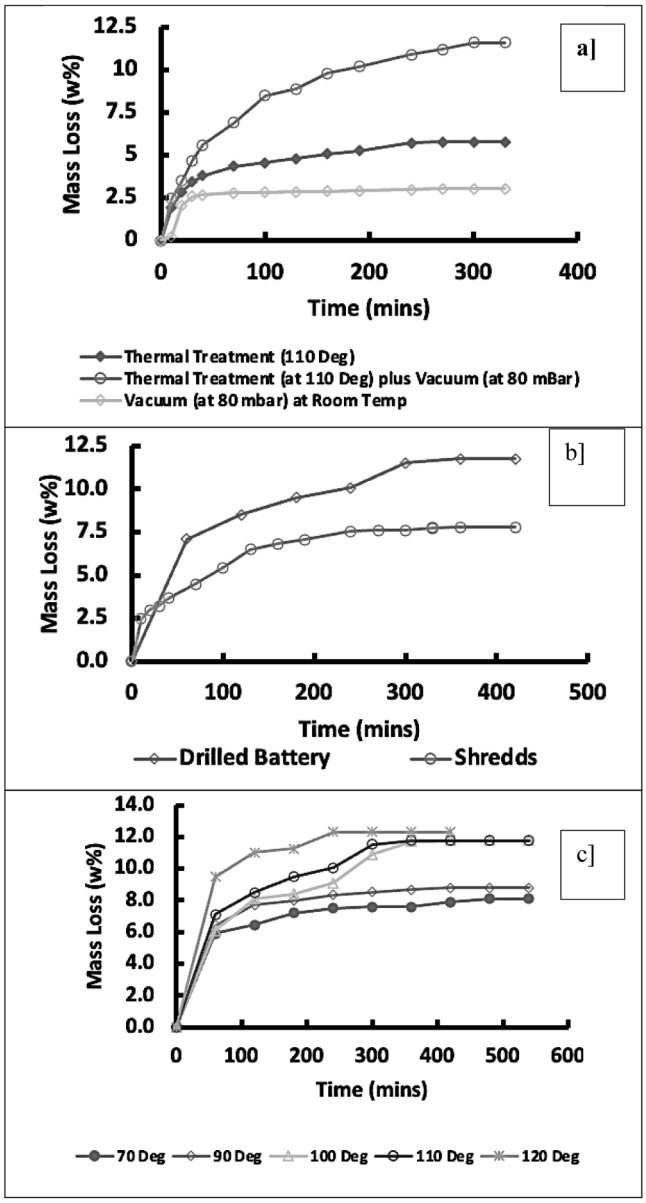

Fig. 6. Effect of temperature on battery weight loss at 80 mBar.

fragments [13]. This contributes further to the observed mass loss but also highlights the risk of over-processing, which can compromise the structural integrity of valuable cell components.

Effect of temperature on solvent recovery

Temperature plays a pivotal role in determining the efficiency and selectivity of solvent recovery during the thermal treatment of spent LFP batteries under vacuum.

At lower temperatures (e.g., at and below 70 °C), the vapour pressure of organic carbonate solvents such as EC, DMC, and EMC remains insufficient to drive effective vaporisation. Consequently, only a small amount of solvent undergoes vaporisation and condensation, resulting in low electrolyte solvent recovery rates of 48 % and below. This limitation is particularly pronounced for EC, which has a higher boiling point and stronger intermolecular interactions due to its cyclic structure.

In contrast, elevating the temperature under vacuum substantially increases the vapour pressure of these solvents, enhancing their volatility and promoting more efficient desorption from the porous electrode matrix. At temperatures exceeding 110 °C, a significant portion of 84 % of the electrolyte solvents is recovered as condensates, indicating that low thermal input can evaporate almost all the electrolyte solvents and overcome the binding energy between the solvents and the solid components of the battery, including the cathode material and binder matrix. The vacuum environment further facilitates this process by reducing the boiling points of the solvents, thus lowering the required thermal energy input for evaporation and minimising oxidative degradation pathways.

However, while higher temperatures improve recovery, they also introduce the risk of thermal decomposition of electrolyte salts such as $LiPF_6$. This decomposition can generate corrosive and hazardous byproducts like HF, POF_3, and PF_5, which not only degrade the recovered solvent purity but can also react with the electrode materials, leading to the formation of inorganic residues such as LiF and phosphate species [13]. These residues are typically confirmed via ATR-FTIR and XRD analyses [31,32],. Additionally, excessive temperatures can cause structural changes in the cathode material and further gas evolution, which may exceed the capacity of the condensation system, reducing liquid recovery.

Therefore, an optimal temperature window exists, typically around 110–120 °C, where solvent recovery is maximised up to 84 % while minimising decomposition of electrolyte components. This balance is critical for enabling high-yield, high-purity recovery of solvents in processes aimed at closed-loop recycling of lithium-ion batteries.

Characterisation of the collected products

The proposed mild-temperature thermal treatment process yielded two distinct products: a light brown liquid and an off-white solid residue, which was deposited on the electrode surfaces. The light brown liquid was collected using a diaphragm pump and low temperature (~20 °C) condensation trapping, while the solid residue formed on the surface of the electrodes. The analysis of these two product phases is detailed below.

Liquid phase – condensate

A significant fraction of the evaporated electrolyte condensed as a light brown liquid at the cooler end of the condensation column, outside the heated zone. This liquid condensate was collected after each thermal run and analysed using ATR-FTIR to identify the retained organic solvents and any decomposition products.

ATR-FTIR spectroscopy of both the battery-drained electrolyte and the thermally recovered condensate revealed characteristic absorption bands attributable to organic carbonate solvents and salt degradation products. In the recovered condensate, peaks consistent with the presence of EC, DMC, DEC, and EMC were observed [2,23,33,34]. The key vibrational bands and corresponding functional groups were identified as follows:

- **C═O stretching** at ~1750 cm^{-1} – carbonyl groups in EC, DMC, DEC
- **C–O–C asymmetric/symmetric stretching** at ~1015 cm^{-1}, 1190 cm^{-1}, 1250 cm^{-1} – ether/ester bonds in linear and cyclic carbonates
- **Alkyl C–H stretching** at ~2850–3000 cm^{-1} – methyl and methylene groups in organic solvents
- **O–H stretching** at ~3500 cm^{-1} – absorbed moisture or trace HF from $LiPF_6$ hydrolysis
- **P–F stretching** at ~910 cm^{-1} – associated with undecomposed $LiPF_6$
- **F–P–F bending** at ~505 cm^{-1} – associated with undecomposed $LiPF_6$
- **P═O stretching** at ~1190 cm^{-1} – from phosphate-based decomposition products (e.g., POF_3, OPF_2)
- **Ring deformation or phosphate species at** ~760 cm^{-1} – likely related to cyclic structures or salt residues

The prominence of carbonate-related peaks, particularly at 1015, 1190, 1250 cm^{-1} (C–O–C stretches) and 1750 cm^{-1} (C═O stretch), in the condensate indicates the recovery of multiple carbonate solvents, including DMC, EMC, and notably EC [6,23,29,33]. Although EC has a

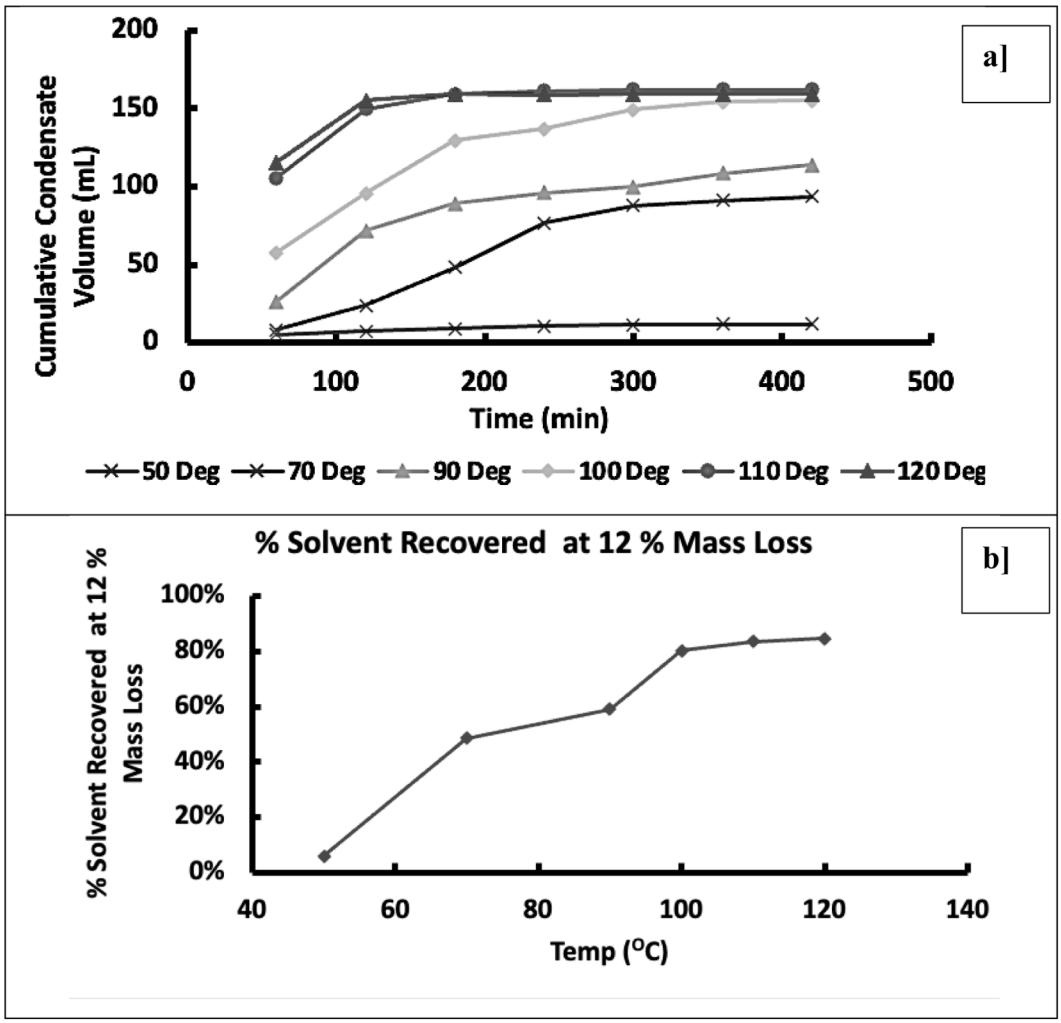

Fig. 7. Effect of temperature on solvent recovery at 80 mBar vacuum pressure.

higher boiling point (~108 °C) compared to DMC (~50 °C) and EMC (~28 °C) at vacuum pressure, its presence in the condensate suggests that under the optimised low-temperature vacuum-assisted distillation conditions employed, partial volatilisation and condensation of EC occurred alongside the more volatile linear carbonates. In contrast, the drained electrolyte displayed more intense bands in the phosphate and fluorinated regions, indicating a greater abundance of salt and its degradation products. Their diminished intensity in the recovered electrolyte solvent fraction implies partial but incomplete removal of these species during thermal treatment and condensation. In addition, the condensate was analysed using IC and no trace contaminants were detected.

Solid phase – white crystals on electrodes

During thermal-vacuum treatment of the electrolyte, portions of the evolved exhaust gases condensed on the cooler walls outside the heated zone, resulting in visible white liquid (Fig. 6). Upon cooling the drilled batteries to room temperature, white deposits rapidly crystallised into solid white crystals deposited on the electrode surfaces. Approximately 0.5 g of this crystalline residue was collected and subjected to ATR-FTIR, XRD, and ICP-OES analysis (Figs. 7 and 9).

The FT-IR spectra of the solid residue obtained after thermal treatment at 110 °C were recorded using the ATR technique. As illustrated in Fig. 8, the predominant vibrational bands are consistent with the presence of $LiPF_6$, evidenced by characteristic absorptions at approximately 980 cm^{-1} (P–F stretching) and 500 cm^{-1} (F–P–F bending) [23]. This suggests minimal decomposition of $LiPF_6$ during the thermal treatment. Additional minor peaks observed at 1050 cm^{-1} and 480 cm^{-1} are attributed to phosphoryl fluoride (POF_3), suggesting partial thermal decomposition of $LiPF_6$ [28]. A distinct feature near 760 cm^{-1} may be associated with phosphate ring deformation modes or residual cyclic phosphate species. The broad absorption around 3500 cm^{-1} likely corresponds to O–H stretching, indicative of trace moisture or hydroxyl-containing species [20].

Furthermore, a band near 1650 cm^{-1} is assigned to asymmetric bending vibrations of CH_2 and CH_3 groups, pointing to the presence of residual organic components. Additional weak bands in the 1050–1300 cm^{-1} region and C–H stretching features around 2900–3000 cm^{-1} further support the presence of trace amounts of organic carbonate solvents. These are most likely remnants of DEC, EMC or EC, which may have co-condensed or partially crystallised with $LiPF_6$ during the heating process [22].

XRD analysis of the residues from 110 °C treatments further confirmed the crystalline nature of the solid phase (Fig. 10).

XRD patterns identified $LiPF_6$ as the dominant crystalline phase, exhibiting characteristic reflections matching its known structure. No peaks aligning with the LiF crystalline phase, which suggests minimal decomposition of $LiPF_6$ during the thermal treatment. Additional weak and broad peaks suggest the presence of solid or semi-crystalline residues, likely from organic solvents.

To determine the elemental composition, the solid condensate was

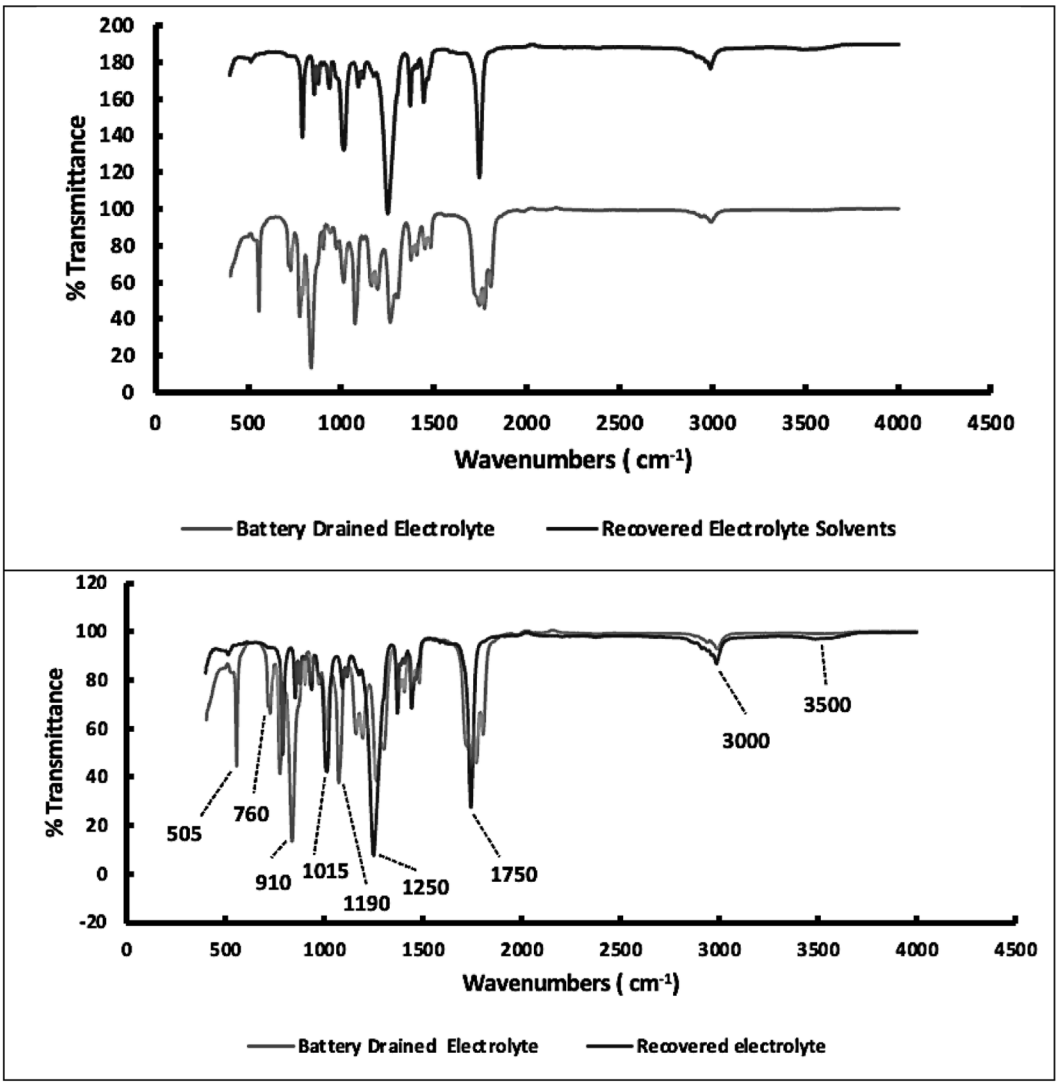

Fig. 8. FTIR of the liquid condensate (electrolyte solvents) at 110 °C, after 300 min at a vacuum pressure of 80 mBar.

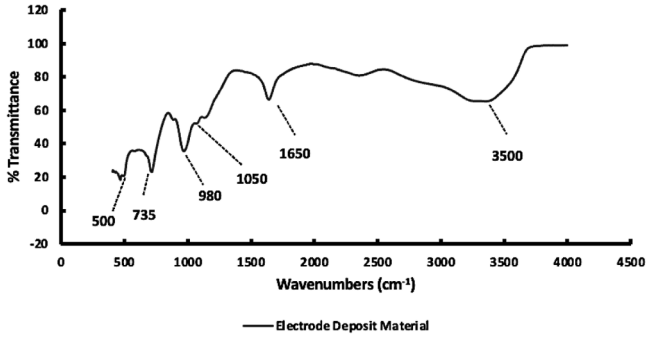

Fig. 9. FTIR pattern of the recovered white crystals after thermal-vacuum treatment for 300 min at 110 °C and 80 mBar vacuum pressure.

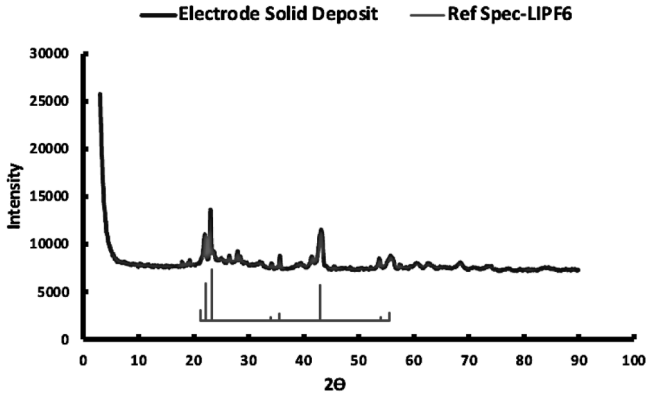

Fig. 10. The XRD pattern of the white crystals obtained after thermal treatment at 110 °C, 80 mBar and 300 min of thermal-vacuum treatment in the range from 0° to 90° 2Θ.

dissolved in 0.5 M HNO_3 and analysed via ICP-OES. Li was measured at 3200 ppm, P was measured at 2300 ppm, along with trace levels of transition metals, including Mn (2.1 ppm), Co (1.85 ppm), Cu (1.1 ppm), Ni (1.5 ppm), and Al (1.1 ppm). These impurities are presumed to originate from residual cathode materials and current collectors in the original electrolyte.

Li is present at elevated levels in the recovered residue because it tends to remain in stable solid forms, such as LiF or as residual $LiPF_6$ that did not fully decompose. During thermal treatment, particularly under vacuum, these lithium-containing compounds are relatively non-volatile and remain in the solid phase. In contrast, P is found at much lower

concentrations because the phosphorus-containing component of the electrolyte, $LiPF_6$, decomposes into volatile byproducts such as POF_3 and PF_5. These gaseous species readily escape under vacuum and elevated temperatures, leading to a net loss of phosphorus from the residue. This difference in thermal stability and volatility explains the observed Li-to-P ratio imbalance in post-treatment samples.

$LiPF_6$ exhibits poor thermal stability and decomposes through different pathways depending on environmental conditions. In dry, inert atmospheres, it thermally breaks down into solid LiF and gaseous PF_5 (Eq. (3)). When moisture is present, PF_5 hydrolyses to form POF_3 and HF (Eq. (3)). However, even trace amounts of water can drive direct decomposition of $LiPF_6$ into LiF, POF_3, and HF (Eq. (5) and 6) [35].

Reported onset temperatures for decomposition vary: Kock et al. [36] identified 134.84 °C for anhydrous $LiPF_6$ and 114.46 °C for its hydrolysis. Notably, in the presence of carbonate solvents (EC, EMC, DMC) and moisture, HF and POF_3 have been detected below 90 °C [34]. Hydrolysis sensitivity to water content is high; for example, degradation was observed at 87 °C with only 300 ppm H_2O [37]. Moisture uptake during cell disassembly, sample preparation, or freezer storage (4 °C) likely triggered the hydrolysis reaction in this study.

Although PF_5's characteristic peaks (1050 cm^{-1} and 950 cm^{-1}) overlap with organic solvent vibrations, its presence cannot be ruled out. Other high-temperature decomposition products of DMC, EMC, and EC, such as CO_2, CO, C_2H_4, and C_2H_6O, were not detected at process temperatures up to 150 °C, suggesting that the solvents were successfully recovered during low-temperature treatment.

Scrubber solution analysis (Volatile species, HF and POF_3 emissions)

Exhaust gases were passed through gas washing bottles to trap volatile byproducts, PF_5, HF and POF_3. HF reacts with water to form aqueous hydrofluoric acid, while POF_3 is easily hydrolysed to yield both HF and H_3PO_4 (phosphoric acid) via the following reactions (Eq. (3)–6). The resulting wash solution had a pH of 6. IC confirmed no presence of F^- and PO_4^{3-} at different retention times, indicating no presence of $LiPF_6$ decomposition products since there wasn't any gas capture and conversion of these gases into hydrofluoric and phosphoric acid, which are potentially recoverable by-products.

The most prominent anions that can be detected were F^- and PF_6^-, their respective absence confirms no partial volatilisation or aerosol transport of $LiPF_6$. F^- signals reflect hydrolysis of PF_6^-, consistent with known reactions:

$$LiPF_6(aq) \rightarrow LiF(s) + PF_5(g) \quad (3)$$

$$HF(g) \xrightarrow{H_2O} HF(aq) \quad (4)$$

$$PF_5(g) + H_2O(l) \rightarrow POF_3(g) + 2HF(g) \quad (5)$$

$$POF_3(g) + 3H_2O(l) \rightarrow 3HF(g) + H_3PO_4(aq) \quad (6)$$

In addition, no $LiPF_6$ decomposition or hydrolysis intermediate species PO_4^{3-}, PO_3F^{2-}, and possibly $PO_2F_2^-$ were detected, indicating no ongoing hydrolysis and secondary reactions.

Environmental and safety implications

Unlike conventional shredding or high-temperature pyrolysis, the low-temperature vacuum-assisted process minimises hazardous emissions and energy utilisation. The FT-IR and IC results highlight the environmental benefit of capturing and neutralising volatile organic compounds and acidic gases, which would otherwise be released in open systems. This method presents a safer, more sustainable alternative for electrolyte recovery in LiB recycling.

Comparison with other electrolyte recovery techniques

Compared to supercritical CO_2 extraction and solvent washing, the vacuum-assisted method operates under milder conditions and requires no additional chemicals. Solvent extraction can yield comparable recovery rates but often involves toxic or flammable reagents and longer processing times. Supercritical methods demand complex infrastructure. The present method offers scalability, safety, and economic feasibility, especially for early-stage recovery.

Conclusion

The study successfully demonstrated that low-temperature vacuum-assisted distillation enables efficient recovery of volatile electrolyte solvents from spent LiBs. Optimal recovery of 84 % occurred at 110 °C and 80 mBar vacuum pressure, yielding DMC, EC and EMC with minimal decomposition of the conductive salt. FT-IR, TGA, XRD, and IC analysis confirmed the composition of the recovered products and environmental safety of the process. Early-stage solvent removal is recommended to minimise electrolyte solvent losses during mechanical recycling and to recover valuable materials in a safer, more environmentally friendly manner.

Funding

Funding provided by the Department of Science and Innovation (DSI) in South Africa in order to execute this research project is gratefully acknowledged. Additionally, financial and strategic support received through the Western Cape Department of Mobility (WCDM) in South Africa is greatly appreciated.

CRediT authorship contribution statement

Tendai Tawonezvi: Writing – review & editing, Writing – original draft, Visualization, Validation, Supervision, Software, Project administration, Methodology, Investigation, Formal analysis, Data curation, Conceptualization. **Anele Sinto:** Writing – review & editing, Validation, Methodology, Investigation, Formal analysis, Conceptualization. **Dorcas Zide:** Writing – review & editing, Validation, Supervision, Methodology, Formal analysis. **Myalelo Nomnqa:** Writing – review & editing, Validation, Methodology, Investigation, Formal analysis. **Bernard J. Bladergroen:** Writing – review & editing, Visualization, Validation, Supervision, Software, Resources, Project administration, Methodology, Investigation, Funding acquisition, Formal analysis, Data curation, Conceptualization.

Declaration of competing interest

The authors declare that they have no known competing financial interests or personal relationships that could have appeared to influence the work reported in this paper.

Acknowledgements

Funding provided by the Department of Science and Innovation (DSI) in South Africa in order to execute this research project is gratefully acknowledged. Additionally, financial and strategic support received through the Western Cape Department of Mobility (WCDM) in South Africa is greatly appreciated.

Data availability

Data will be made available on request.

References

[1] A. Yoshino, The birth of the lithium-ion battery, Angew. Chem. Int. Ed. 51 (2012) 5798–5800, https://doi.org/10.1002/anie.201105006.
[2] H. Zhang, H. Zhao, M.A. Khan, W. Zou, J. Xu, L. Zhang, J. Zhang, Recent progress in advanced electrode materials, separators and electrolytes for lithium batteries, J. Mater. Chem. A 6 (2018) 20564–20620, https://doi.org/10.1039/C8TA05336G.

[3] C.M. Costa, E. Lizundia, S. Lanceros-Méndez, Polymers for advanced lithium-ion batteries: state of the art and future needs on polymers for the different battery components, Prog. Energy Combust. Sci. 79 (2020) 100846, https://doi.org/10.1016/j.pecs.2020.100846.
[4] T. Tawonezvi, D. Zide, M. Nomnqa, L. Petrik, B.J. Bladergroen, Selective electrodeposition of Co-Ni alloys from synthetic quasi LiB NMC 532 cathode sulphate solutions using rotating plate potentiostatic electrowinning, Chem. Eng. J. Adv. 17 (2024) 100579, https://doi.org/10.1016/j.ceja.2023.100579.
[5] Dong, L., Sun, X., Sun, L., Zhao, D., Wang, C., Gong, W.T., Fang, M.M., Wang, P., Zhang, H., Lei, Z., Xie, Y., You, F.: A comprehensive analysis on EU batteries regulation: lifecycle decarbonization, business challenge and compliance risk, (2025).
[6] S. Lee, H. Koo, H.S. Kang, K.-H. Oh, K.W. Nam, Advances in polymer binder materials for lithium-ion battery electrodes and separators, Polymers 15 (2023) 4477, https://doi.org/10.3390/polym15234477.
[7] D. Das, S. Manna, S. Puravankara, Electrolytes, additives and binders for NMC cathodes in Li-ion batteries—a review, Batteries 9 (2023) 193, https://doi.org/10.3390/batteries9040193.
[8] Cattaneo, P., D'Aprile, F., Kapelyushko, V., Mustarelli, P., Quartarone, E.: Supercritical CO2 technology for the treatment of end-of-life lithium ion batteries, (2024).
[9] D. Mu, Y. Liu, R. Li, Q. Ma, C. Dai, Transcritical CO2 extraction of electrolytes for lithium-ion batteries: optimization of the recycling process and quality–quantity variation, New J. Chem. 41 (2017) 7177–7185, https://doi.org/10.1039/C7NJ00771J.
[10] K. He, Z.-Y. Zhang, L. Alai, F.-S. Zhang, A green process for exfoliating electrode materials and simultaneously extracting electrolyte from spent lithium-ion batteries, J. Hazard. Mater. 375 (2019) 43–51, https://doi.org/10.1016/j.jhazmat.2019.03.120.
[11] L. Bläubaum, P. Röse, F. Baakes, U. Krewer, Impact of lithium-ion battery separators on gas evolution during temperature abuse, Batter. Supercaps. 7 (2024), https://doi.org/10.1002/batt.202300534.
[12] E.R. Logan, H. Hebecker, A. Eldesoky, A. Luscombe, M.B. Johnson, J.R. Dahn, Performance and degradation of LiFePO4 /graphite cells: the impact of water contamination and an evaluation of common electrolyte additives, J. Electrochem. Soc. 167 (2020) 130543, https://doi.org/10.1149/1945-7111/abbbbe.
[13] N. Zachmann, M. Petranikova, B. Ebin, Electrolyte recovery from spent Lithium-Ion batteries using a low temperature thermal treatment process, J. Ind. Eng. Chem. 118 (2023) 351–361, https://doi.org/10.1016/j.jiec.2022.11.020.
[14] D. Zhang, L. Ding, T. Wu, F. Yang, F. Lan, Y. Cao, M. Xiang, Facile preparation of a lithium-ion battery separator with thermal shutdown function based on polypropylene/polyethylene microsphere composites, Ind. Eng. Chem. Res. 60 (2021) 18530–18539, https://doi.org/10.1021/acs.iecr.1c04271.
[15] Y. Duan, L. Guo, Q. Zhou, H. Wang, L. Zhang, F.-N. Shi, Preparation of degradable polycarbonate from low boiling point organic matter of waste electrolyte, J. Mater. Cycles. Waste Manage. 26 (2024) 1119–1130, https://doi.org/10.1007/s10163-024-01889-8.
[16] I.T. Adebanjo, J. Eko, A.G. Agbeyegbe, S.F. Yuk, S.V. Cowart, E.A. Nagelli, F. J. Burpo, J.L. Allen, D.T. Tran, N. Bhattarai, K. Shah, J.-Y. Hwang, H.H. Sun, A comprehensive review of lithium-ion battery components degradation and operational considerations: a safety perspective, Energy Adv. (2025), https://doi.org/10.1039/D5YA00065C.
[17] L.A. Gomez-Moreno, A. Klemettinen, R. Serna-Guerrero, A simple methodology for the quantification of graphite in end-of-life lithium-ion batteries using thermogravimetric analysis, IScience 26 (2023) 107782, https://doi.org/10.1016/j.isci.2023.107782.
[18] S. Solchenbach, M. Metzger, M. Egawa, H. Beyer, H.A. Gasteiger, Quantification of PF5 and POF3 from side reactions of LiPF6 in Li-ion batteries, J. Electrochem. Soc. 165 (2018) A3022–A3028, https://doi.org/10.1149/2.0481813jes.
[19] J. Alvarado, M.A. Schroeder, M. Zhang, O. Borodin, E. Gobrogge, M. Olguin, M. S. Ding, M. Gobet, S. Greenbaum, Y.S. Meng, K. Xu, A carbonate-free, sulfone-based electrolyte for high-voltage Li-ion batteries, Mater. Today 21 (2018) 341–353, https://doi.org/10.1016/j.mattod.2018.02.005.
[20] E. Bingöl, A.T. Erciyes, Styrenated oil synthesis with cyclic carbonate functional groups on polystyrene segment, Polymers 13 (2021) 2343, https://doi.org/10.3390/polym13142343.
[21] A.K. Das, K. Sunanda, B.N. Rajasekhar, Electronic and vibrational spectroscopy of ethyl methyl carbonate: a comparative experimental and theoretical study, J. Quant. Spectrosc. Radiat. Transf. 272 (2021) 107789, https://doi.org/10.1016/j.jqsrt.2021.107789.
[22] D. Aurbach, B. Markovsky, A. Shechter, Y. Ein-Eli, H. Cohen, A comparative study of synthetic graphite and Li electrodes in electrolyte solutions based on ethylene carbonate-dimethyl carbonate mixtures, J. Electrochem. Soc. 143 (1996) 3809–3820, https://doi.org/10.1149/1.1837300.
[23] K. Xu, Nonaqueous liquid electrolytes for lithium-based rechargeable batteries, Chem. Rev. 104 (2004) 4303–4418, https://doi.org/10.1021/cr030203g.
[24] K. Xu, Nonaqueous liquid electrolytes for lithium-based rechargeable batteries, Chem. Rev. 104 (2004) 4303–4418, https://doi.org/10.1021/cr030203g.
[25] J. Dodwell, M. Maier, J. Majasan, R. Jervis, L. Castanheira, P. Shearing, G. Hinds, D.J.L. Brett, Open-circuit dissolution of platinum from the cathode in polymer electrolyte membrane water electrolysers, J. Power. Sources 498 (2021) 229937, https://doi.org/10.1016/j.jpowsour.2021.229937.
[26] Y. Ikezawa, H. Nishi, In situ FTIR study of the Cu electrode/ethylene carbonate+dimethyl carbonate solution interface, Electrochim. Acta 53 (2008) 3663–3669, https://doi.org/10.1016/j.electacta.2007.12.038.
[27] M. Cai, M.S. Ruthkosky, B. Merzougui, S. Swathirajan, M.P. Balogh, S.H. Oh, Investigation of thermal and electrochemical degradation of fuel cell catalysts, J. Power. Sources 160 (2006) 977–986, https://doi.org/10.1016/j.jpowsour.2006.03.033.
[28] S.E. Sloop, J.B. Kerr, K. Kinoshita, The role of Li-ion battery electrolyte reactivity in performance decline and self-discharge, J. Power. Sources 119–121 (2003) 330–337, https://doi.org/10.1016/S0378-7753(03)00149-6.
[29] Y. Akita, M. Segawa, H. Munakata, K. Kanamura, In-situ fourier transform infrared spectroscopic analysis on dynamic behavior of electrolyte solution on LiFePO4 cathode, J. Power. Sources 239 (2013) 175–180, https://doi.org/10.1016/j.jpowsour.2013.03.134.
[30] Han, J.Y., Jung, S.: Thermal stability and the effect of water on hydrogen fluoride generation in lithium-ion battery electrolytes containing LiPF6. Batteries 8, 61 (2022). https://doi.org/10.3390/batteries8070061.
[31] Y. Jiang, C. Peng, K. Zhou, H. Zhou, T. Chen, G. Zhang, W. Chen, Impact and removal of fluorine impurity in the comprehensive recovery of spent LiFePO4/C, Sep. Purif. Technol. 362 (2025) 131766, https://doi.org/10.1016/j.seppur.2025.131766.
[32] H. Yang, G.V. Zhuang, P.N. Ross, Thermal stability of LiPF6 salt and Li-ion battery electrolytes containing LiPF6, J. Power. Sources 161 (2006) 573–579, https://doi.org/10.1016/j.jpowsour.2006.03.058.
[33] C. Wu, Y. Bai, F. Wu, Fourier-transform infrared spectroscopic studies on the solid electrolyte interphase formed on Li-doped spinel Li1.05Mn1.96O4 cathode, J. Power. Sources 189 (2009) 89–94, https://doi.org/10.1016/j.jpowsour.2008.11.016.
[34] A. Iizuka, E. Shibata, Mass spectrometric study on volatilization behavior of electrolyte solvents of lithium-ion batteries, Mater. Trans. 62 (2021) 1030–1038, https://doi.org/10.2320/matertrans.M-M2021824.
[35] E.W.C. Spotte-Smith, T.B. Petrocelli, H.D. Patel, S.M. Blau, K.A. Persson, Elementary decomposition mechanisms of lithium hexafluorophosphate in battery electrolytes and interphases, ACS Energy Lett. 8 (2023) 347–355, https://doi.org/10.1021/acsenergylett.2c02351.
[36] M.D.S. Lekgoathi, B.M. Vilakazi, J.B. Wagener, J.P. Le Roux, D. Moolman, Decomposition kinetics of anhydrous and moisture exposed LiPF6 salts by thermogravimetry, J. Fluor. Chem. 149 (2013) 53–56, https://doi.org/10.1016/j.jfluchem.2013.02.011.
[37] B.S. Ndazi, S. Karlsson, Characterization of hydrolytic degradation of polylactic acid/rice hulls composites in water at different temperatures, Express. Polym. Lett. 5 (2011) 119–131, https://doi.org/10.3144/expresspolymlett.2011.13.